# Crystal structure of the BRCT repeat region from the breast cancer-associated protein, BRCA1

R. Scott Williams, Ruth Green and J. N. Mark Glover

Department of Biochemistry

University of Alberta

Edmonton, Alberta

T6G 2H7

Correspondence should be addressed to J.N.M.G.

email: mark.glover@ualberta.ca

**Summary**

The C-terminal, BRCT region is essential to the DNA repair, transcriptional regulation and tumor suppressor functions of BRCA1. The crystal structure of the human BRCA1 BRCT domain has now been determined at 2.5 Å resolution. The domain contains two BRCT repeats, which adopt similar structures and are packed together in a head-to-tail arrangement. Cancer-causing missense mutations occur at the interface between the two repeats and destabilize the structure. The manner by which the two BRCT repeats interact in BRCA1 may represent a general mode of interaction between homologous domains within proteins that interact to regulate the cellular response to DNA damage. The structure provides a basis to predict the structural consequences of previously uncharacterized BRCA1 mutations.

The C-terminal region in BRCA1 is essential to its tumor suppressor activity because missense and truncation mutations within this region lead to early onset breast cancer[1-4]. This region contains two ~90-100 amino acid sequence repeats called BRCT (**BR**CA1 **C**-**t**erminal) repeats[5,6], which bear weak amino acid sequence similarity to other proteins involved in DNA repair, such as the yeast protein RAD9, the mammalian protein XRCC1, as well as the p53 binding protein, 53BP1. BRCT repeats are thought to serve as multi-purpose protein-protein interaction modules, binding to other BRCT repeats or other protein domains with apparently unrelated structures. A large body of evidence suggests that the BRCA1 BRCT region interacts with proteins involved in transcriptional control or DNA repair, including the transcriptional co-repressor CtIP, histone deacetylases, p53, p300, and the DNA damage-associated helicase BACH1[7] (for a review, see[8]).

**Domain mapping and structure determination**

We set out to determine the X-ray structure of the BRCT region of BRCA1 to gain structural insights into its function and to provide a basis to assess the cancer risks associated with specific BRCT mutations. We first used limited proteolytic mapping to locate a folded protein domain within a purified C-terminal fragment of human BRCA1 (residues 1528-1863). As shown in Fig. 1, both trypsin and elastase rapidly digest BRCA1(1528-1863) to a proteolytically stable fragment. Electrospray mass spectrometry and N-terminal sequencing of the

products of the trypsin digestion indicated that the major species had a molecular weight of 25038 (+/- 5) Da and the N-terminal sequence “VNKR”, corresponding to BRCA1 residues 1646-1863. This fragment contains both BRCT repeats[5,6], which suggests that the two BRCT repeats and the associated linker together form a stable structural unit. Deletion of residues 1860-1863, which are not conserved in the other mammalian homologues of BRCA1, yielded a highly soluble fragment, BRCA1(1646-1859). We crystallized and determined the structure of BRCA1(1646-1859) at 2.5 Å resolution using the multiwavelength anomalous dispersion method (MAD)[9] and a seleno-methionine substituted BRCT derivative (Fig. 2*a-c*, Table 1).

**Overall structure**

The dual-repeat, BRCT domain of BRCA1 adopts an elongated structure ~70 Å long and ~30-35 Å in diameter. Each of the two BRCT repeats adopts a structure similar to that previously observed in the isolated, C-terminal BRCT repeat from XRCC1[10], as well as the single BRCT repeat in an $NAD^+$-dependent DNA ligase[11]. The BRCT fold is characterized by a central parallel four-stranded $\beta$-sheet with a pair of $\alpha$-helices ($\alpha$1 and $\alpha$3) packed against one face and a single $\alpha$-helix ($\alpha$2) packed against the opposite face of the sheet (Fig. 2*a,b*). A structural alignment of the two BRCA1 BRCT repeats with the XRCC1 repeat (Fig. 2*d*) reveals that the relative arrangement of $\alpha$1, $\alpha$3 and the central $\beta$-sheet is conserved in all three repeats. However, the conformations of the $\beta$1-$\alpha$1, $\beta$2-$\beta$3 and $\beta$3-$\alpha$2 connecting loops, as well as the orientation of $\alpha$2 relative to the central

β-sheet, are much less conserved. The conservation of the α1-α3-β-sheet structure is maintained by the packing of a limited number of key conserved hydrophobic residues in the core of the BRCT fold[10].

**BRCT repeat interactions**

The two BRCT repeats in BRCA1 interact in a head-to-tail fashion, burying ~1600 Å$^2$ of hydrophobic, solvent accessible surface area in the interface (Fig. 3*a-c*). The core of this interface is formed by the interaction of three α helices: α2 of the N-terminal repeat and α1' and α3' from the C-terminal repeat. The residues in these helices that contribute to the inter-repeat interface are almost all hydrophobic, and pack tightly in a knobs-into-holes manner. The 23 amino acid linker connecting the two BRCT repeats is poorly defined in the electron density, possibly indicating flexibility. It is clear, however, that the central portion of the linker is helical (αL) and packs against the C-terminal base of the α2-α1'-α3' helical bundle. The only salt bridge across the interface occurs between Arg 1699, immediately N-terminal to α2, and a pair of acidic residues, Glu 1836 and Asp 1840, exposed on the surface of α3'.

Multiple, tandem BRCT repeats are common in many of the BRCT-containing proteins such as 53BP1, RAD9, RAD4, DNA ligase IV, XRCC1, and the topoisomerase II binding protein TOPBP1. An amino acid sequence alignment of the two BRCA1 BRCT repeats with those in 53BP1 and RAD9 reveals that the residues that occupy the interface between the two repeats in α2, α1' and α3' of BRCA1 are highly conserved in 53BP1 and RAD9 (Fig. 3*d*). This

observation strongly suggests that the two BRCT repeats in 53BP1 and RAD9 also pack via a triple helical interface similar to that seen in BRCA1. Sequence alignments in the $\alpha$2 regions of the other BRCT-containing proteins are less reliable, due to the low level of sequence similarity between these proteins in this region. Nevertheless, many of these proteins show significant conservation of interface residues in $\alpha$1' and $\alpha$3', suggesting that this mode of packing could be common within the BRCT family. In proteins with more than two BRCT repeats, such as RAD4, the DNA polymerase II subunit Dpb11, and TOPBP1, this kind of packing could result in long, rod-like protein structures, whose surfaces would consist of the BRCT repeat loops and the highly variable inter-repeat linker peptides. Such elongated structures could provide a scaffold for the regulated assembly of multi-protein complexes.

Individual BRCT repeats have also been found to interact in *trans* with the BRCT repeats of other proteins. For example, the C-terminal BRCT repeat in the DNA repair protein XRCC1 has been shown to interact with the DNA ligase III BRCT repeat[12]. While it is tempting to speculate that such interactions may occur through interactions between $\alpha$2 of one protein and the $\alpha$1/$\alpha$3 face of the other, recent evidence suggests that XRCC1-DNA ligase III BRCT interactions involve residues exposed on the surface of $\alpha$1 in both proteins[13]. Structural studies of other BRCT-BRCT complexes, as well as an analysis of the effects of surface exposed mutations on the ability of BRCT proteins to associate and carry out their function *in vivo,* will be required to further test structural models of heteromeric BRCT-BRCT interactions.

**BRCT mutations**

The structure of the BRCT region of BRCA1 provides a powerful tool to interpret the large database of mutations that have been found in this domain in breast and ovarian cancer patients. For example, a nonsense mutation at Tyr 1853 deletes the last 11 amino acids of the second BRCA1 BRCT domain and is associated with early-onset breast cancer[3]. The peptide corresponding to the deleted residues normally adopts an extended conformation which packs against $\alpha$2' and the $\beta$–sheet of the C-terminal BRCT repeat. Three hydrophobic residues within the deleted region, Tyr 1853, Leu 1854 and Ile 1855, are conserved in other BRCT repeats and are packed in the hydrophobic core of the C-terminal BRCT repeat. We predict that the deletion of these residues should destabilize the protein fold.

Two missense mutations within the BRCT region, Ala 1708 → Glu, and Met 1775 → Arg, are linked to breast and ovarian cancer[1,2]. These mutations cripple the DNA double-strand break repair function of BRCA1 in human cells[14]. They also block the ability of the BRCT domain to interact with CtIP[15,16], histone deacetylases[17] and BACH1[7] and to activate transcription[18]. Ala 1708 and Met 1775 are part of the hydrophobic contact surface between the two BRCT repeats (Fig. 3*a*-*c*). Ala 1708 in $\alpha$2 packs into a small hydrophobic pocket formed by $\alpha$1' and $\alpha$3' near the center of the interface, which would not be expected to accommodate the larger, negatively charged Glu at position 1708. Met 1775 is packed within a predominantly hydrophobic pocket near the edge of the inter-

repeat interface. Substitution of this residue with an Arg could be sterically accommodated but would position the positive charge near another basic residue, Arg 1835. We therefore predict that these mutations destabilize the hydrophobic inter-repeat interface and could lead to a repositioning of the repeats relative to one another, or, potentially, the complete unfolding of the structure.

To test directly the structural consequences of these mutations, we assayed the sensitivity of dual-repeat BRCT domain proteins harboring these mutations to proteolytic degradation (Fig. 4*a*). Both wild type and mutant proteins were produced by *in vitro* transcription/translation because the Tyr 1853 → *stop* and Ala 1708 → Glu mutants were insoluble when expressed in *E. coli*. The wild type protein is highly resistant to digestion by trypsin, elastase, or chymotrypsin, indicating that the *in vitro* produced BRCT protein is stably folded. In contrast, the Tyr 1853 → *stop* and Ala 1708 → Glu mutants are almost completely degraded by low concentrations of all enzymes, indicating that these proteins are not stably folded under the assay conditions. The Met 1775 → Arg mutant displays an intermediate sensitivity to proteolytic degradation, suggesting that the Met 1775 → Arg mutant exhibits a subtler structural defect.

The cancer risks associated with the vast majority of BRCA1 missense mutations deposited in the BIC database[19] are unknown. Using our structure, we predict several of these mutations will seriously impair the folding of the BRCT domain, and will therefore lead to an elevated cancer risk (Fig. 4*b*). Such mutations include non-conservative substitutions of key hydrophobic residues packed in the protein core or mutations that disrupt electrostatic interactions.

Many mutations remain unclassified, such as mutations in the hydrophobic core that replace one hydrophobic residue with another of significantly smaller or larger size. While such mutations can be accommodated in highly stable proteins such as lysozyme through a subtle re-packing of the hydrophobic core[20], similar mutations may be more detrimental in the less stable BRCA1 BRCT domain. Finally, many mutations occur on the surface of the structure, and are not predicted to alter the fold of the BRCT domain, but may nevertheless perturb a binding site for an important BRCT partner. The analysis of the biochemical and *in vivo* effects of such surface mutations could provide strong evidence for the involvement of specific BRCT-interacting proteins in BRCA1 function and tumor suppression.

## Methods

### BRCT expression and purification

Human BRCA1(1528-1863), used in the initial domain mapping experiments, was expressed and purified as a GST-fusion protein by glutathione-affinity chromatography. BRCA1(1528-1863) was then cleaved from GST using Prescission protease (Amersham-Pharmacia) and the C-terminal BRCA1 polypeptide was purified from GST by anion exchange chromatography.

Human BRCA1(1646-1859), used for crystallization, was expressed as an untagged recombinant protein in *E.coli* strain BL21(DE3). Purification was achieved using a combination of ammonium sulfate precipitation, hydrophobic interaction, anion exchange and gel filtration chromatography.

### Proteolytic mapping of the BRCT domain

Purified BRCA1(1528-1863) at 400 μg/mL was digested with either elastase (50 μg $mL^{-1}$) or trypsin (2 μg $mL^{-1}$) for the indicated times (Fig. 1), the reactions were terminated with PMSF, and the reaction products were separated by SDS-PAGE and stained with Coomassie.

To assay the proteolytic sensitivity of BRCT domain mutants, wild type BRCA1 BRCT (1646-1859), as well as Ala 1708 → Glu, Met 1775 → Arg and Tyr 1853 → *stop* mutants were expressed by *in vitro* transcription/translation (TNTQuick, Promega) and labeled with $^{35}$S-methionine. The transcription/translation reactions were centrifuged to remove insoluble material. Three μL of the supernatant from each reaction was then digested with either

trypsin, elastase or chymotrypsin for 10 minutes at 25 $^{o}$C in a final reaction volume of 15 μL. Reaction products were visualized by SDS-PAGE and autoradiography.

**Crystallization**

Crystals were grown at 20-23 $^{o}$C using the hanging drop vapor diffusion technique. Crystals of seleno-methionine-substituted BRCA1(1646-1859) were grown by mixing 3 μL of 20 mg mL$^{-1}$ BRCT domain in protein solution (400 mM NaCl, 5 mM Tris-HCl pH 7.5) with 3 μL of well solution 1 (1.5 M $(NH4)_2SO_4$, 100 mM MES, pH 6.7, 10 mM $CoCl_2$) (Table 1). Native crystals were grown by mixing 3 μL 18 mg mL$^{-1}$ BRCA1(1646-1859) in protein solution with 3 μL well solution 2 (0.8 M $LiSO_4$, 100 mM Tris-HCl, pH 8.5, 2.5 mM $NiCl_2$, 5 mM $CaCl_2$).

**Data collection and processing**

For data collection at 100 K, crystals were flash frozen in liquid nitrogen after gradual transfer to a cryoprotectant solution comprised of the respective well solution supplemented with 26% glycerol. MAD and native data were obtained at beamlines 14BM-D and 14BM-C, respectively, at the Advanced Photon Source (APS, BioCARS). All data were scaled and reduced with the HKL package[21].

**Phasing, model building and refinement**

Eight of nine selenium positions were located and refined using SOLVE[9],

and crystallographic phases were improved by solvent flattening and histogram matching implemented in DM[22]. The majority of the polypeptide chain was built with O[23] using the solvent-flattened, MAD-phased electron density map at 2.9 Å resolution. The initial model was first refined against the remote wavelength ($\lambda 3$) MAD dataset to 2.9 Å resolution in CNS[24] using torsion angle molecular dynamics (MLHL target). Maximum likelihood targets, bulk solvent correction and overall anisotropic B-factor scaling were applied throughout the refinement process. Further refinement against the native data to 2.5 Å resolution involved iterative cycles of manual building and restrained refinement with TLS group anisotropic thermal parameter modeling as implemented in REFMAC (v5.0.32)[25,26]. Anomalous difference Fourier synthesis using the native data and phases calculated from the final model, confirmed the positions of 10/13 sulphur atoms and a single nickel atom in the asymmetric unit. Poor electron density was observed for much of the inter-repeat linker and the $\beta$3-$\alpha$2 and $\beta$3'-$\alpha$2' loops, suggesting that these regions are relatively flexible. As a result, linker residues 1743-1747 have been modeled as poly-alanine, while residues 1692 and 1693 from the $\beta$3-$\alpha$2 loop and residues 1817-1819 from the $\beta$3'-$\alpha$2' loop have been omitted from the final model. Analysis of stereochemistry by PROCHECK[27] indicates that the model contains 82.8% of the residues in the most favorable regions of the Ramachandran plot, with no residues in the disallowed regions. Refinement statistics are provided in Table 1. Figures were created with BOBSCRIPT[28] and rendered with RASTER3D[29] (Fig. 3*b,c*), or POVRAY[30] (Fig. 2*a-d*, Fig. 3*a*).

## Atomic coordinates

Coordinates are currently being submitted to the protein data bank.

## Acknowledgements

We would like to thank Luc Gaudreau for the gift of the BRCA1(1568-1863) expression plasmid and helpful discussions, Brian Mark and Jason Lamoureux for help with x-ray data collection and Keith Brister and the staff of APS BioCARS for excellent technical support during synchrotron data collection. This work was supported by operating grants from the Canadian Institutes of Health Research, the Canadian Breast Cancer Research Initiative and the Alberta Heritage Foundation for Medical Research.

## References


1. Miki, Y. *et al. Science* **266**, 66-71 (1994).
2. Futreal, P.A. *et al. Science* **266**, 120-122 (1994).
3. Friedman, L.S. *et al. Nat. Genet.* **8**, 399-404 (1994).
4. Gayther, S.A. *et al. Am. J. Hum. Genet.* **58**, 451-456 (1996).
5. Koonin, E.V., Altschul, S.F.& Bork, P. *Nat. Genet.* **13**, 266-268 (1996).
6. Callebaut, I.& Mornon, J.P. *FEBS Lett.* **400**, 25-30 (1997).
7. Cantor, S.B. *et al. Cell* **105**, 149-160 (2001).
8. Deng, C.X.& Brodie, S.G. *Bioessays* **22**, 728-737 (2000).
9. Terwilliger, T.C.& Berendzen, J. *Acta Crystallogr.* **D 55 (Pt 4)**, 849-861 (1999).
10. Zhang, X. *et al. EMBO J.* **17**, 6404-6411 (1998).
11. Lee, J.Y. *et al. EMBO J.* **19**, 1119-1129 (2000).
12. Nash, R.A., Caldecott, K.W., Barnes, D.E.& Lindahl, T. *Biochemistry* **36**, 5207-5211 (1997).
13. Dulic, A. *et al. Biochemistry* **40**, 5906-5211 (2001).
14. Scully, R. *et al. Mol. Cell* **4**, 1093-1099 (1999).
15. Yu, X., Wu, L.C., Bowcock, A.M., Aronheim, A.& Baer, R. *J. Biol. Chem.* **273**, 25388-25392 (1998).
16. Li, S. *et al. J. Biol. Chem.* **274**, 11334-8 (1999).
17. Yarden, R.I.& Brody, L.C. *Proc. Natl. Acad. Sci. U S A* **96**, 4983-4988 (1999).
18. Chapman, M.S.& Verma, I.M. *Nature* **382**, 678-679 (1996).
19. http://www.nhgri.nih.gov/Intramural_research/Lab_transfer/Bic/
20. Eriksson, A.E. *et al. Science* **255**, 178-183 (1992).

21. Otwinowski, Z.& Minor, W. *Methods Enzymol.* **276**, 307-325 (1997).

22. Cowtan , K. *Joint CCP4 and ESF-EACBM Newsletter on Protein Crystallography* **31**, 34-38 (1994).

23. Jones, T.A., Zou, J.Y., Cowan, S.W.& Kjeldgaard *Acta Crystallogr.* **A 47 ( Pt 2)**, 110-119 (1991).

24. Brünger, A.T. *et al. Acta Crystallogr.* **D 54**, 905-921 (1998).

25. Collaborative Computational Project, N.4. *Acta Crystallogr.* **D 50**, 760-763 (1994).

26. Winn, M.D., Isupov, M.N.& Murshudov, G.N. *Acta Crystallogr.* **D 57**, 122-133 (2001).

27. Laskowski, R.A., MacArthur, M.W.& Thornton, J.M. *Curr. Opin. Struct. Biol.* **8**, 631-639 (1998).

28. Kraulis, P.J. *J. Applied Crystallogr.* **24**, 946-950 (1991).

29. Merritt, E.A.& Bacon, D.J. *Methods Enzymol.* **277**, 505-524 (1997).

30. Persistence of Vision Ray Tracer v.3.02, Copyright 1997 POV-Team. www.

povray. Org

**Figure legends**

**Fig. 1.** The two BRCT repeats form a single protein domain. BRCA1(1528-1863) was digested with either trypsin or elastase for the times indicated, and the products were analysed by SDS-PAGE. The open arrows indicate BRCA1(1528-1863), the closed arrows indicate the proteolytically resistant fragments.

**Fig 2.** ***a*****,** The structure of the dual-repeat BRCT domain of BRCA1. The secondary structure elements in the C-terminal BRCT repeat are labeled "prime" to distinguish them from the corresponding secondary structure elements in the N-terminal repeat. ***b,*** C$\alpha$ backbone trace of the BRCA1 BRCT domain. The N-terminal BRCT repeat is colored turquoise, the C-terminal repeat is gold and the inter-repeat linker is colored gray. The view is rotated $90^{o}$ clockwise from the view shown in *a*. ***c*****,** MAD-phased electron density at 2.9 Å resolution and contoured at 1.0 $\sigma$ is displayed for the inter-BRCT repeat interface. ***d,*** A stereoview of a structural alignment of the N- and C-terminal BRCA1 BRCT repeats and the C-terminal BRCT repeat from XRCC1[10]. Least squares alignments were produced using O[23].

**Fig 3.** The packing of BRCT repeats. In *a*-*c*, the N-terminal repeat is colored turquoise, the C-terminal repeat gold, and residues that cause cancer when mutated are red. ***a*****,** Three helices interact to form the core of the BRCT repeat

interface (stereoview). ***b*****,** An electrostatic surface representation of the C-terminal BRCT repeat is displayed with a worm representation of $\alpha$2 from the N-terminal repeat. ***c*****,** An electrostatic surface representation of the N-terminal repeat is shown with a worm representation of $\alpha$1' and $\alpha$3' from the C-terminal repeat. ***d*****,** An amino acid sequence alignment of the regions of BRCA1, 53BP1 and RAD9 that are predicted to form BRCT-BRCT interfaces. Residues that constitute this interface in BRCA1, as well as conserved residues in h53BP1 and *S. cerevisia*e RAD9 are colored green. Residues where cancer-causing missense mutations have been identified are boxed in red.

**Fig 4.** Analysis of the structural consequences of mutations in the BRCT domain. ***a*****,** $^{35}$S-methionine-labelled wild type BRCA1(1646-1859), as well as variants harboring the indicated mutations were digested with the indicated proteases and the reaction products were analysed by SDS-PAGE and autoradiography. Reactions were carried out at elastase concentrations of 0, 3, 30 and 300 $\mu$g mL$^{-1}$ (lanes 1-4), trypsin concentrations of 0, 6, 60 and 600 $\mu$g mL$^{-1}$ (lanes 5-8), and chymotrypsin concentrations of 0, 6, 60 and 600 $\mu$g mL$^{-1}$ (lanes 9-12). ***b*****,** Missense mutations in the human BRCA1 BRCT domain. Missense mutations derived from the BIC[19] are indicated below the BRCT amino acid sequence and the Tyr 1853 → stop mutation is indicated with an X. Mutations with predicted deleterious effects on folding are colored red. Mutations known to cause cancer are boxed. Residues in green are involved in the inter-BRCT repeat interface.

**Table 1: X-ray data collection, phasing and refinement statistics**

**Data Collection**

| | | | | | |
|---|---|---|---|---|---|
| Data set | | Native | | MAD | |
| Space group | | $P6_122$ | | $P6_122$ | |
| Cell dimensions | a=b(Å) | 114.44 | | 114.39 | |
| | c (Å) | 122.11 | | 121.38 | |
| | | | λ1 | λ2 | λ3 |
| Wavelength (Å) | | 1.00 | 0.9793 | 0.9789 | 0.9563 |
| Resolution range (Å) | | 40-2.5 | 20-2.9 | 20-2.9 | 20-2.9 |
| Observations[1] | | 209,566 | 81,799 | 78,519 | 83,902 |
| Unique reflections[1] | | 16,968 | 21,866 | 21,894 | 21,928 |
| Data coverage total/final shell[2] (%) | | 99.8 /100 | 99.7/100 | 99.6/100 | 99.6/100 |
| $<I/\sigma I>$ total/final shell | | 43.2/9.1 | 22.3/4.3 | 21.7/4.0 | 22.2/4.0 |
| $R_{sym}$ total/final shell (%)[3] | | 4.8/29.2 | 4.7/26.5 | 4.7/27.0 | 4.9/30.1 |

| **Refinement Statistics** | | | **Phasing Statistics** | |
|---|---|---|---|---|
| Resolution range(Å) | | 25-2.5 | Resolution range(Å) | 20.0-2.9 |
| $R_{work}/R_{free}$ (%)[4] | | 25.9/30.2 | No. of Selenium Sites | 8/9 |
| No. of refined atoms | Protein | 1548 | FOM – Solve | 0.64 |
| | Water | 123 | | |
| | Nickel | 1 | | |
| R.m.s. deviations | Bonds (Å) | 0.017 | | |
| | Angles (°) | 1.81 | | |
| Average B-factors(Å$^2$) | Protein | 37.8 | | |
| | Water | 47.6 | | |

[1] For MAD datasets, Bijvoets (I+ and I-) were kept separate during scaling and for calculation of statistics.

[2] Final shell: 2.57 – 2.50 Å (native); 3.02 – 2.90 Å (MAD)

[3] $R_{sym}=\Sigma |(I_{hkl}) - <I>| / \Sigma(I_{hkl})$ where $I_{hkl}$ is the integrated intensity of a given reflection.

[4] $R_{work} = \Sigma_h|F_o(h) – F_c(h)| / \Sigma_h | F_o(h)|$, where $F_o(h)$ and $F_c(h)$ are observed and calculated structure factors. $R_{free}$ calculated with 5% of all reflections excluded from refinement stages using the native data set. No $I/\sigma I$ cutoff was used in the refinement.

**Fig. 1**

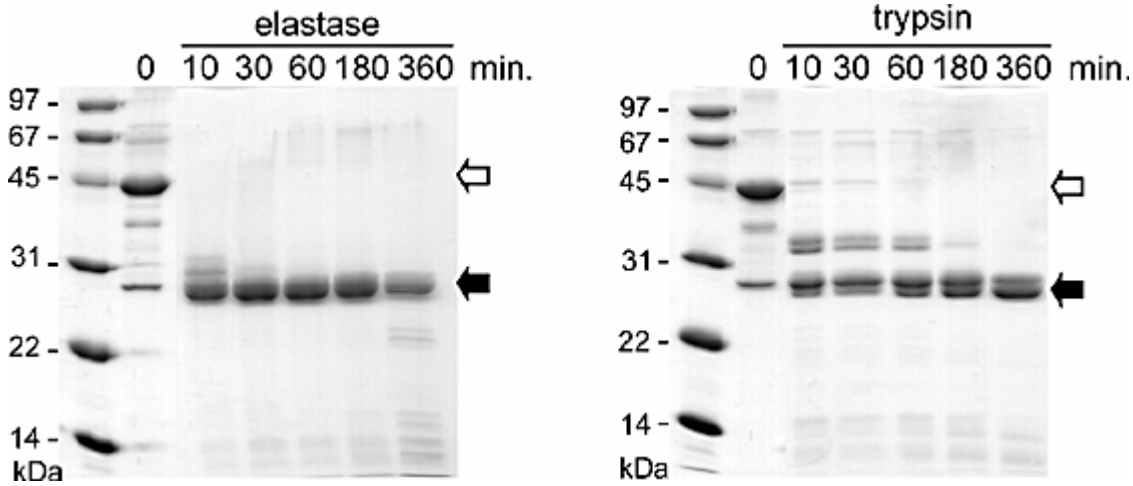
elastase
0 10 30 60 180 360 min.
97 -
67 -
45 -
31 -
22 -
14 -
kDa
trypsin
0 10 30 60 180 360 min.
97 -
67 -
45 -
31 -
22 -
14 -
kDa

**Fig. 2**

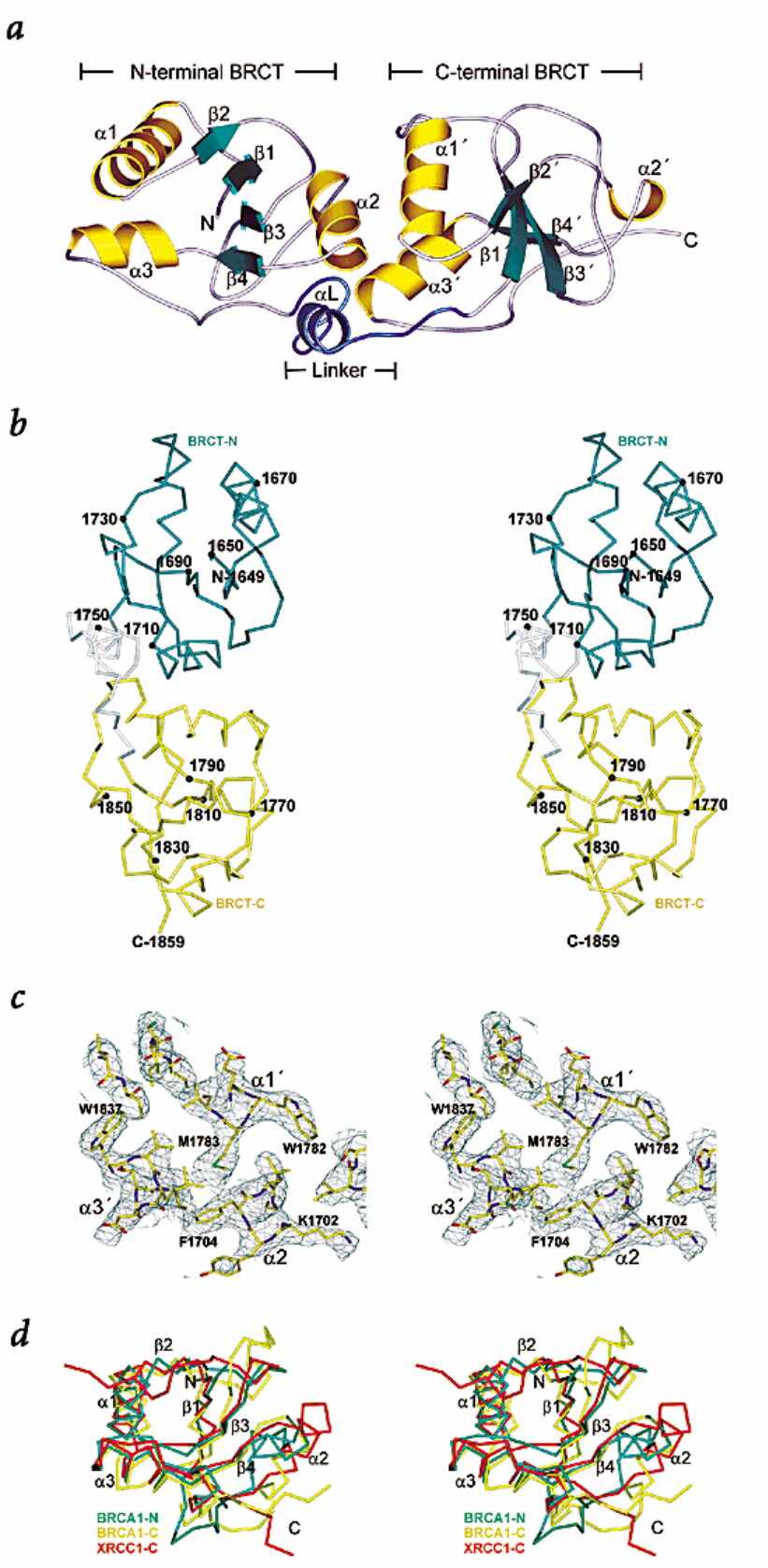
a
N-terminal BRCT
C-terminal BRCT
α1
β2
β1
α2
N
β3
α3
β4
αL
Linker
α1´
β2´
α2´
β4´
C
β1´
β3´
α3´
b
BRCT-N
1670
1730
1650
1690
N-1649
1750
1710
1790
1850
1810
1770
1830
BRCT-C
C-1859
c
α1´
W1837
M1783
W1782
α3´
K1702
F1704
α2
d
β2
N
α1
β1
β3
β4
α2
α3
C
BRCA1-N
BRCA1-C
XRCC1-C

**Fig. 3.**

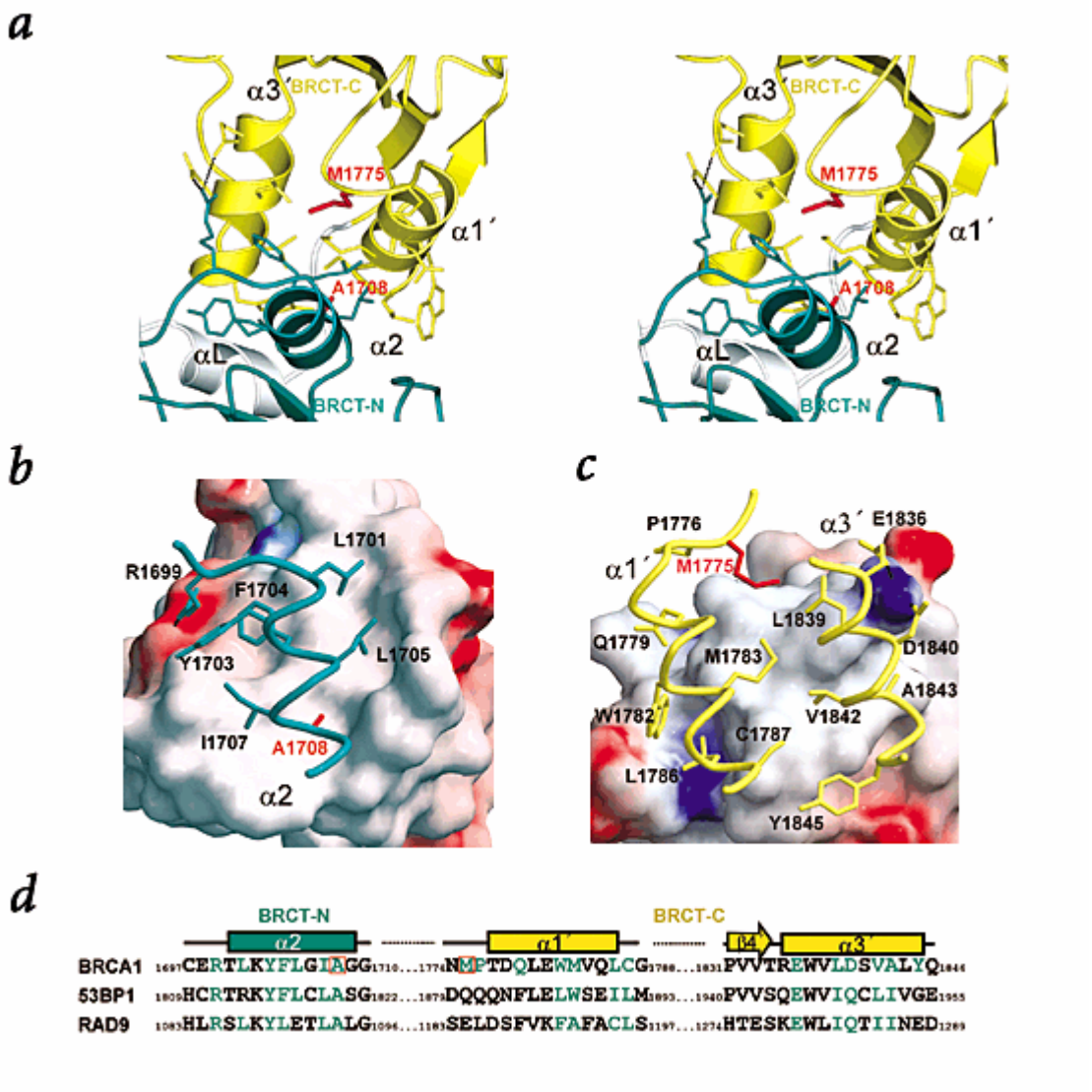
a
α3´
BRCT-C
M1775
α1´
A1708
αL
α2
BRCT-N
b
L1701
R1699
F1704
Y1703
L1705
I1707
A1708
α2
c
P1776
α3´
E1836
α1´
M1775
L1839
Q1779
M1783
D1840
A1843
W1782
V1842
C1787
L1786
Y1845
d
BRCT-N
BRCT-C
α2
α1´
β4
α3´
BRCA1 1697CERTLKYFLGIAGG1710...1774NMPTDQLEWMVQLCG1788...1831PVVTREWVLDSVALYQ1844
53BP1 1809HCRTRKYFLCLASG1822...1879DQQQNFLELWSEILM1893...1940PVVSQEWVIQCLIVGE1955
RAD9 1083HLRSLKYLETLALG1096...1183SELDSFVKFAFACLS1197...1274HTESKEWLIQTIINED1289

**Fig. 4.**

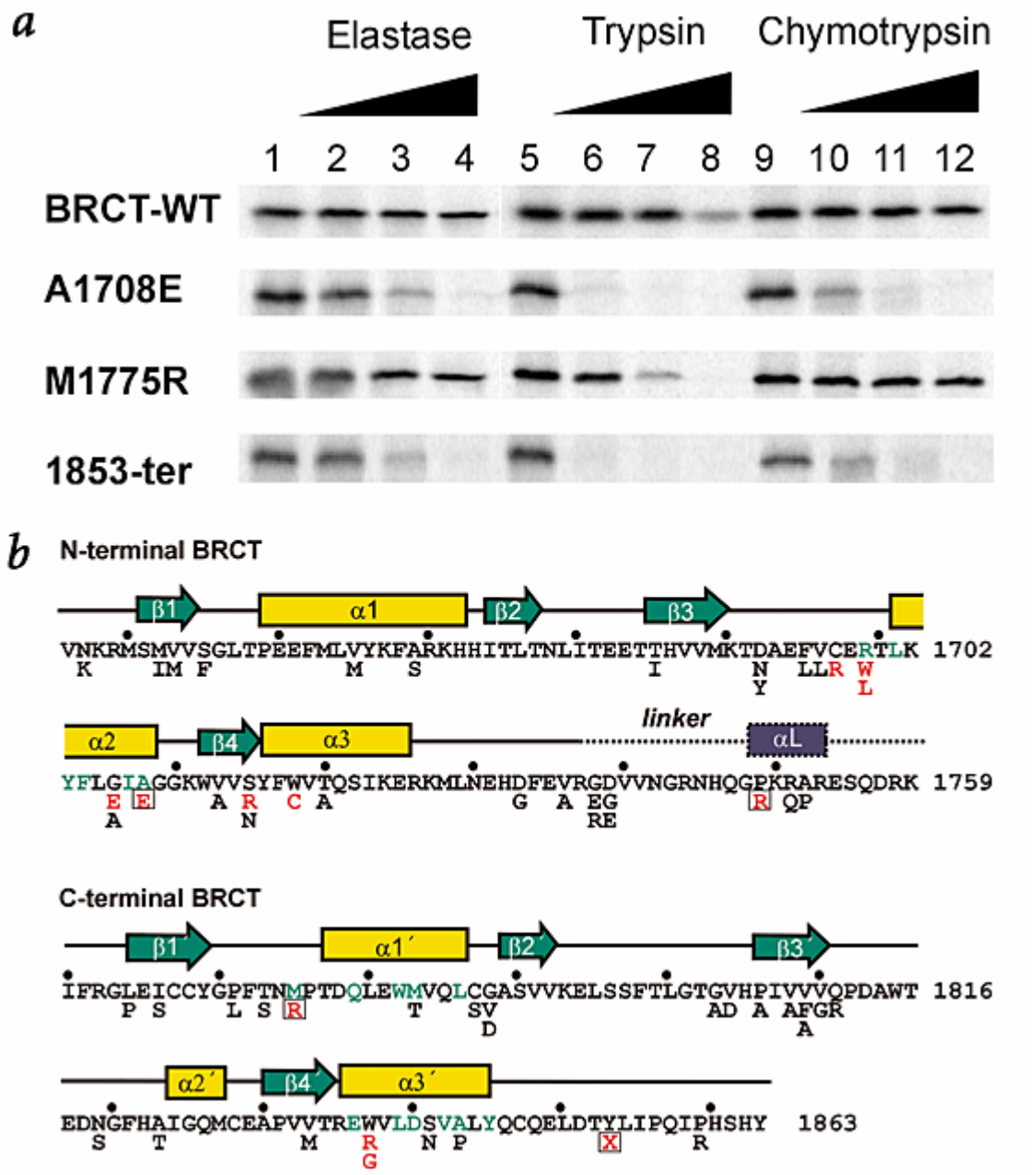
a
Elastase
Trypsin
Chymotrypsin
1 2 3 4 5 6 7 8 9 10 11 12
BRCT-WT
A1708E
M1775R
1853-ter
b
N-terminal BRCT
β1 α1 β2 β3
VNKRMSMVVSGLTPEEFMLVYKFARKHHITLTNLITEETTHVVMKTDAEFVCERTLK 1702
K IM F M S I N LLR W
Y L
α2 β4 α3 linker αL
YFLGIAGGKWVVSYFWVTQSIKERKMLNEHDFEVRGDVVNGRNHQGPKRARESQDRK 1759
E E A R C A G A EG R QP
A N RE
C-terminal BRCT
β1´ α1´ β2´ β3´
IFRGLEICCYGPFTNMPTDQLEWMVQLCGASVVKELSSFTLGTGVHPIVVVQPDAWT 1816
P S L S R T SV AD A AFGR
D A
α2´ β4´ α3´
EDNGFHAIGQMCEAPVVTREWVLDSVALYQCQELDTYLIPQIPHSHY 1863
S T M R N P X R
G